

ATT3D: Amortized Text-to-3D Object Synthesis

Jonathan Lorraine Kevin Xie Xiaohui Zeng Chen-Hsuan Lin Towaki Takikawa
Nicholas Sharp Tsung-Yi Lin Ming-Yu Liu Sanja Fidler James Lucas
NVIDIA Corporation

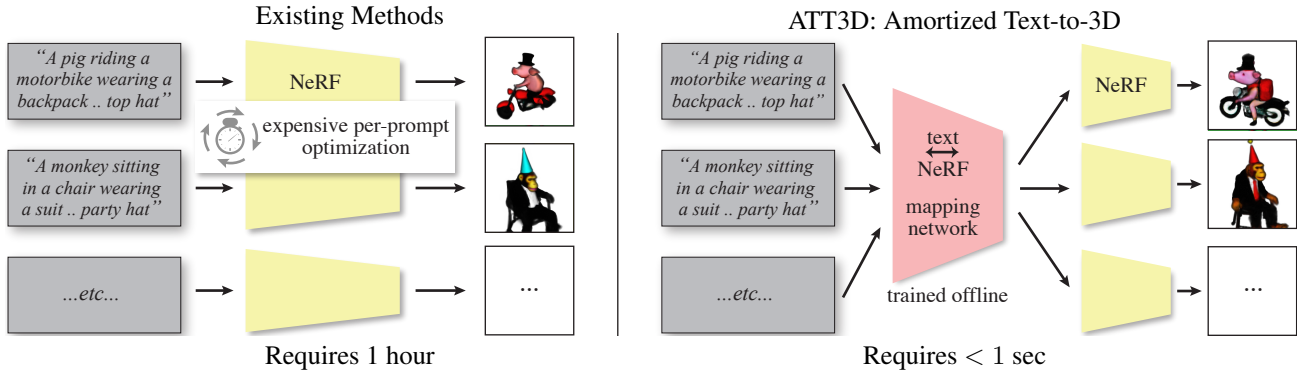


Figure 1: Our method initially trains one network to output 3D objects consistent with various text prompts. After, when we receive an unseen prompt, we produce an accurate object in < 1 second, with 1 GPU. Existing methods re-train the entire network for every prompt, requiring a long delay for the optimization to complete. Further, we can interpolate between prompts for user-guided asset generation (Fig. 3). We include a [project webpage](#) with an overview and videos.

Abstract

Text-to-3D modelling has seen exciting progress by combining generative text-to-image models with image-to-3D methods like Neural Radiance Fields. DreamFusion recently achieved high-quality results but requires a lengthy, per-prompt optimization to create 3D objects. To address this, we amortize optimization over text prompts by training on many prompts simultaneously with a unified model, instead of separately. With this, we share computation across a prompt set, training in less time than per-prompt optimization. Our framework – Amortized text-to-3D (ATT3D) – enables knowledge sharing between prompts to generalize to unseen setups and smooth interpolations between text for novel assets and simple animations.

1. Introduction

3D content creation is important because it allows for more immersive and engaging experiences in industries such as entertainment, education, and marketing. However, 3D design is challenging due to technical complexity of the 3D modeling software, and the artistic skills required to create high-quality models and animations. Text-to-3D (TT3D) generative tools have the potential to democratize 3D content creation by relieving these limitations. To make this technology successful, we desire tools that provide fast responses to users while being inexpensive for the operator.

Recent TT3D methods [1, 2] allow users to generate high-quality 3D models from text-prompts but use a lengthy (~ 15 minute to > 1 hour [1, 2]) per-prompt optimization. Having users wait between each iteration of prompt engineering results in a sporadic and time-consuming design process. Further, generation for a new prompt requires multiple GPUs and uses large text-to-image models [3–5], creating a prohibitive cost for the pipeline operator.

We split the TT3D process into two stages. First, we optimize one model offline to generate 3D objects for many different text prompts simultaneously. This *amortizes optimization* over the prompts, by sharing work between similar instances. The second, user-facing stage uses our amortized model in a simple feed-forward pass to quickly generate an object given text, with no further optimization required.

Our method, Amortized text-to-3D (ATT3D), produces a model which can generate an accurate 3D object in < 1 second, with only 1 consumer-grade GPU. This TT3D pipeline can be deployed more cheaply, with a real-time user experience. Our offline stage trains the ATT3D model significantly faster than optimizing prompts individually while retaining or even surpassing quality, by leveraging compositionality in the parts underlying each 3D object. We also gain a new user-interaction ability to interpolate between prompts for novel asset generation and animations.

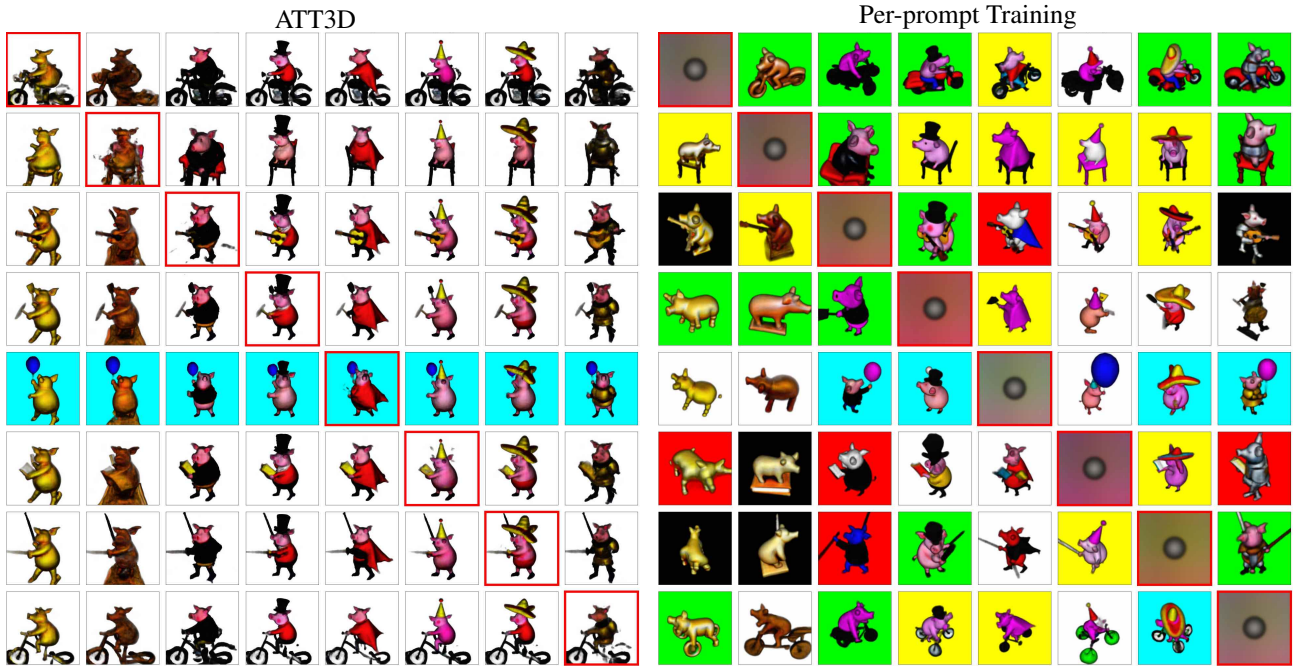


Figure 2: We show results on a compositional prompt set. Each row has a different activity, while each column has a theme, which we combine into the prompt “a pig {activity} {theme}.” while we evaluate generalization on a held-out set of unseen testing prompts in red on the diagonal. *Left:* Our method. Interestingly, the amortized objects have a unified orientation. *Right:* The per-prompt training baseline [1], with a random initialization for unseen prompts to align compute budgets. **Takeaway:** Our model performs comparably to per-prompt training on the seen prompts, with a far smaller compute budget (Fig. 6). Importantly, we perform strongly on **unseen prompts** with no extra training, unlike per-prompt training.

Rendered frames from ATT3D with text embedding $(1 - \alpha)c_1 + \alpha c_2$ for $\alpha \in [0, 1]$

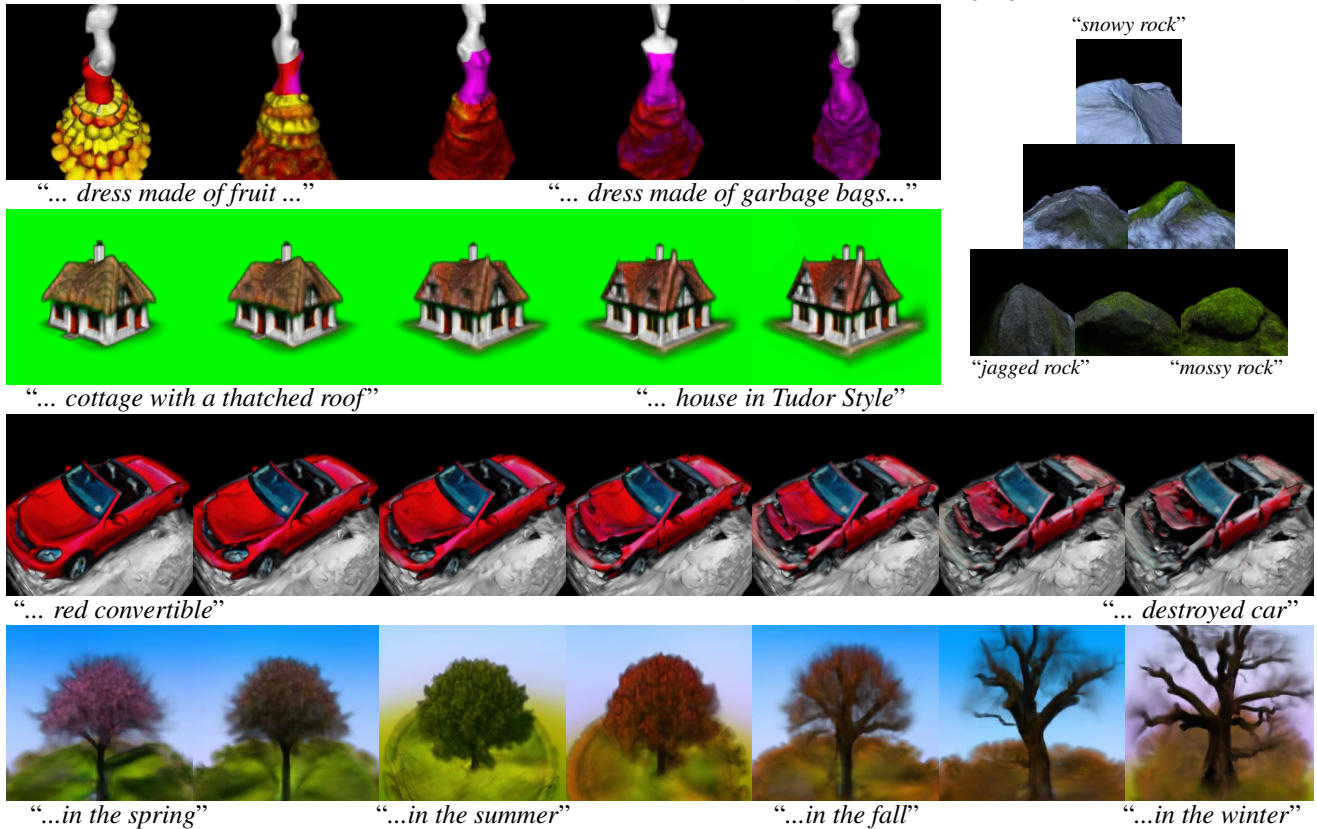


Figure 3: We show renders of our model’s output on interpolated text embeddings $(1 - \alpha)c_1 + \alpha c_2$. We generate a continuum of landscape, clothing, building, and vehicle assets, and use chains of prompts for animations, like seasonality in a tree.

1.1. Contributions

We present a method to synthesize 3D objects from text prompts immediately. By using amortized optimization we can:

- Generalize to new prompts – Fig. 2.
- Interpolate between prompts – Fig. 3.
- Amortize over settings other than text prompts – Sec. 3.2.2.
- Reduce overall training time – Fig. 6.

2. Background

This section contains concepts and prior work relevant to our method, with notation in App. Table 1.

2.1. NeRFs for Image-to-3D

NeRFs [6] represent 3D scenes via a radiance field parameterized by a neural network. We denote 3D coordinates with $\mathbf{x} = [x, y, z] \in \mathcal{X}$ and the radiance values with $\mathbf{r} = [\sigma, r, g, b] \in \mathcal{R}$. NeRFs are trained to output radiance fields to render frames similar to multi-view images with camera information. Simple NeRFs map locations \mathbf{x} to radiances \mathbf{r} via an MLP-parameterized function. Recent NeRFs use spatial grids storing parameters queried per location [7–9], integrating spatial inductive biases. We view this as a *point-encoder* function $\gamma_w: \mathcal{X} \rightarrow \Gamma$ with parameters w encoding a location \mathbf{x} before the final MLP $\nu: \Gamma \rightarrow \mathcal{R}$.

$$\mathbf{r} = \nu(\gamma_w(\mathbf{x})) \quad (1)$$

2.2. Text-to-Image Generation

The wide availability of captioned image datasets has enabled the development of powerful text-to-image generative models. We use a DDM with comparable architecture to recent large-scale methods [3–5]. We train for score-matching, where (roughly) input images have noise added to them [10, 11] that the DDM predicts. Critically, these models can be conditioned on text to generate matching images via classifier-free guidance[12]. We use pre-trained T5-XXL [13] and CLIP [14] encoders to generate text embeddings, which the DDM conditions on via cross-attention with latent image features. Crucially, we reuse the text token embeddings – denoted c – for modulating our NeRF.

2.3. Text-to-3D (TT3D) Generation

Prior works rely on per-prompt optimization to generate 3D scenes. Recent TT3D methods [1, 15] use text-to-image generative models to train NeRFs. To do so, they render a view and add noise. The DDM, conditioned on a text prompt, approximates ϵ with $\hat{\epsilon}$, using the difference $\hat{\epsilon} - \epsilon$ to update NeRF parameters. We outline this method in Alg. 1 and Fig. 4 and refer to DreamFusion Sec. 3 for more details.

2.4. Amortized Optimization

Amortized optimization methods use learning to predict solutions when we repeatedly solve similar instances of the same problem [16]. Current TT3D independently optimizes prompts, whereas, in Sec. 3, we use amortized methods.

A typical amortization strategy is to find a problem context – denoted z – to change our optimization, with some strategies specialized for NeRFs [17]. For example, concatenating the context to the NeRF’s MLP: $\mathbf{r}(\mathbf{x}, z) = \nu(\gamma(\mathbf{x}), z)$ Or, having a *mapping network* m outputting modulations to the weights or hidden units:

$$\mathbf{r}(\mathbf{x}, z) = \nu(\gamma_{m(z)}(\mathbf{x})) \quad (2)$$

But, designing useful contexts, z , can be non-trivial.

3. Our Method: Amortized Text-to-3D

Our method has an initial training stage using amortized optimization, after which we perform cheap inference on new prompts. We first describe the ATT3D architecture and its use during inference, then the training procedure.

3.1. The Amortized Model used at Inference

At inference, our model consists of a *mapping network* m , a NeRF ν , and a spatial grid of features γ_w with parameters w (Fig. 4). The mapping network takes in an (encoded) text prompt c and produces feature grid *modulations*: $\gamma_{m(c)}$. Our final NeRF module ν is a small MLP acting on encoded points $\gamma_{m(c)}(\mathbf{x})$ – Eq. 1 – representing a 3D object for the text prompt with the modulated feature grid. Full details are in App. Sec. B.1 and summarized here. **Architectural details:** We followed Instant NGP [7] for our NeRF, notably using multi-resolution voxel/hash grids for our point-encoder γ . We use hypernetwork modulations for implementation and computational simplicity, with alternatives of concatenation and attention considered in App. B.1.3. Hypernetwork approaches output the point-encoder parameters w from a text embedding c :

$$w = \text{Hypernetwork}(c) \quad (3)$$

We simply output via a vector v from the text embeddings, which is used to output the parameters via linear maps.

$$v = \text{SiLU}(\text{linear}_{w/\text{bias}}^{\text{spec.norm}}(\text{flatten}(c))) \quad (4)$$

$$w = \text{reshape}(\text{linear}_{\text{no bias}}^{\text{spec.norm}}(v)) \quad (5)$$

This w parameterizes the point-encoder γ_w , which is used to evaluate radiances per-point as per Eq. 1. This simple approach solved our prompt sets, so we used it in all results. Using more sophisticated hypernetworks performed comparably but was slower. However, this may be necessary for scaling to more complicated sets of prompts.

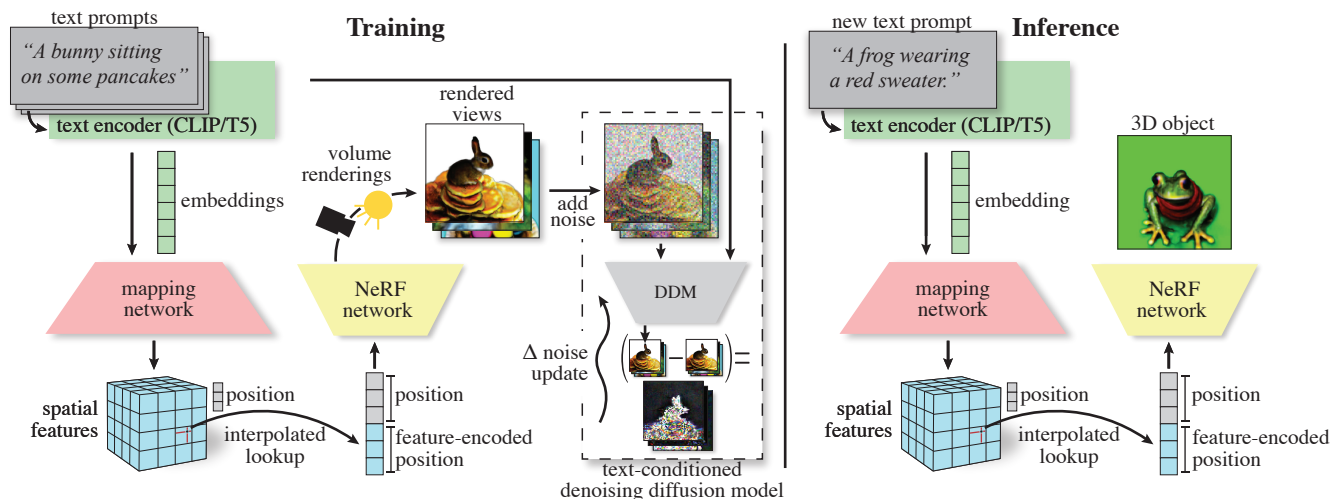


Figure 4: We show a schematic of our text-to-3D pipeline with changes from DreamFusion’s pipeline [1] shown in red and pseudocode in Alg. 1. The text encoder (in green) provides its – potentially cached – text embedding c to the text-to-image DDM and now also to the mapping network m (in red). We use a spatial point-encoder $\gamma_{m(c)}$ (in blue) for our position x , whose parameters are modulations from the mapping network $m(c)$. The final NeRF MLP ν outputs a radiance r given the point encoding: $r = \nu(\gamma_{m(c)}(x))$, which we render into views. *Left*: At training time, the rendered views are input to the DDM to provide a training update. The NeRF network ν , mapping network m , and (effectively) the spatial point encoding $\gamma_{m(c)}$ are optimized. *Right*: At inference time, we use the pipeline up to the NeRF for representing the 3D object.

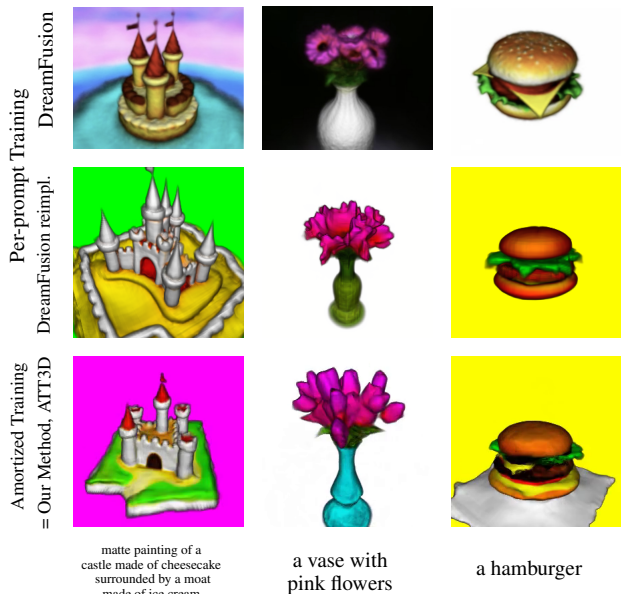


Figure 5: Here we qualitatively assess our method relative to the baseline per-prompt training – i.e., DreamFusion’s method. A public DreamFusion implementation is not available. **Takeaway**: Our re-implementation achieves similar quality to the original. Also, our amortized method performs comparably to per-prompt training.

Designing larger prompt sets was challenging because the per-prompt baselines could not effectively handle open-domain text prompts. We partially overcame this limitation by creating compositional prompt sets using prompt components that the underlying model effectively handled.

3.2. Amortized Text-to-3D Training

Alg. 1 overviews our training procedure. In each optimization step, we sample several prompts and produce their – potentially cached – text embeddings z , which we use to compute the modulations $m(c)$. We also sample camera poses and rendering conditions. These are combined with the NeRF module to render our images. We then use the Score Distillation Sampling loss [1] to update the NeRF.

As in prior work, we augment text prompts depending on camera position – “..., front/side/rear view”. We provide the text embeddings (without augmentation) to the mapping network to modulate the NeRF.

3.2.1 Stabilizing Optimization

The NeRF’s loss is specified by a denoising diffusion model (DDM) and thus changes during training akin to bilevel setups like GANs [18–20] and actor-critic models [21]. We use techniques from nested optimization to stabilize training motivated by observing similar failure modes. Specifically, we required spectral normalization [19] – crucial for large-scale GANs [20] – to mitigate numerical instability.

Removing optimization momentum helped minimize oscillations from complex dynamics as in nested optimization [22, 23]. Unlike DreamFusion, we did not benefit from Distributed Shampoo [24] and, instead, use Adam [25].

3.2.2 Amortizing Over Other Settings

So far, we described amortizing optimization over many prompts. More generally, we can amortize over other variables like the choice of guidance weight, regularizers, data augmentation, or other aspects of the loss function. We use this to explore techniques for allowing semantically meaningful prompt interpolations, which is a valuable property of generative models like GANs [18] and VAEs [26].

There are various prompt interpolation strategies we can amortize over, like, between text embeddings, guidance weights, or loss functions; see App. Fig. 18 for specifics. To sample an interpolated setup, we sample prompt (embedding) pairs c_1, c_2 and an interpolant weight $\alpha \in [0, 1]$. We must give this information to our mapping network - ex., by making it an input $m(c_1, c_2, \alpha)$. Instead, we input interpolated embeddings, allowing an unmodified architecture and incorporating prompt permutation invariance.¹

$$m((1 - \alpha)c_1 + \alpha c_2) \quad (6)$$

In addition to the text prompts distribution, we must choose the interpolant weights α 's distribution. For example, we could sample uniform $\alpha \in [0, 1]$, or a binary $\alpha \in \{0, 1\}$ - i.e., training without interpolants - which are both special cases of a Dirichlet distribution. The Dirichlet concentration coefficient is another user choice to change results qualitatively - see App. Fig. 19. We show examples of various loss interpolations in Figs. 3 and 20. The interpolation setup is further details in App. Sec. B.1.14.

3.3. Why We Amortize

Reduce training cost (Fig. 6): We train on text prompts for a fraction of the per-prompt cost.

Generalize to unseen prompts (Fig. 2, 8): We seek strong performance when evaluating our model on unseen prompts during the amortized training without extra optimization.

Prompt interpolations (Fig. 3): Unlike current TT3D, we can interpolate between prompts, allowing: (a) generating a continuum of novel assets, or (b) creating 3D animations.

4. Results and Discussion

Here, we investigate our method's potential benefits. We refer to the baseline as "per-prompt optimization", which follows existing works using separate optimization for each prompt. The specific NeRF rendering and SDS loss implementation are equivalent between the baseline and our method - see Fig. 5. App. Sec. C contains additional experiments, ablations, and visualizations.

¹By invariance we actually mean $m(c_1, c_2, \alpha) = m(c_2, c_1, 1 - \alpha)$.

Algorithm 1 ATT3D Pseudocode for each update

Changes from DreamFusion Sec. 3 shown in red

```
1: for each loss term in batch do
2:   sample a text and its embedding  $c$ 
3:   compute the modulation  $m' = m(c)$ 
4:   sample camera position
5:   add front/side/back to text, given camera
6:   sample textureless/shadeless/full render
7:   perform the render:
8:     create a ray for each pixel in the frame
9:     at each ray, sample multiple points  $x$ 
10:    at each point, compute encoding  $\gamma' = \gamma_{m'}(x)$ 
11:    at each point, compute the radiance  $\nu(\gamma')$ 
12:    composite radiance into a frame
13:   add noise to frame
14:   compute denoised frame with the DDM via  $\hat{\epsilon}$ 
15:   compute gradient using  $\hat{\epsilon} - \epsilon$  as per SDS
```

4.1. How We Evaluate ATT3D

We first describe the datasets we use, then our metrics for quality and cost.

4.1.1 Our Text Prompt Datasets

DreamFusion (DF): The DF27 dataset consists of the 27 prompts from DreamFusion's main paper, while DF411 has 411 prompts from the project page. We explore memorizing these datasets but find them unsuitable for generalization.

Compositional: To test generalization, we design a compositional prompt set by composing fragments with the template " a {animal} {activity} {theme}" and hold out a subset of "unseen" prompts. Our model must generalize to unseen compositions that require nontrivial changes to geometry. Using this template, we created a small pig-prompts and a larger animal-prompts dataset detailed in App. Sec. B.1.12 and shown in Figs. 2 and 8. We hold out 8 out of the 64 pig prompts, as shown in Fig. 2. For the animals, the held-out prompts are sampled homogeneously and we investigate holding out larger fractions of the prompts.

4.1.2 Our Evaluation Metrics

Cost: We measure the computational cost of training per-prompt models versus our amortized approach. Wall-clock time and number of iterations are insufficient because we train with varying compute setups and numbers of GPUs - see App. Sec. B.2. To account for this difference, we measure the number of rendered frames used for training (normalized by the number of prompts). Specifically, this is the number of optimization iterations times batch size divided by the total number of prompts in the dataset.

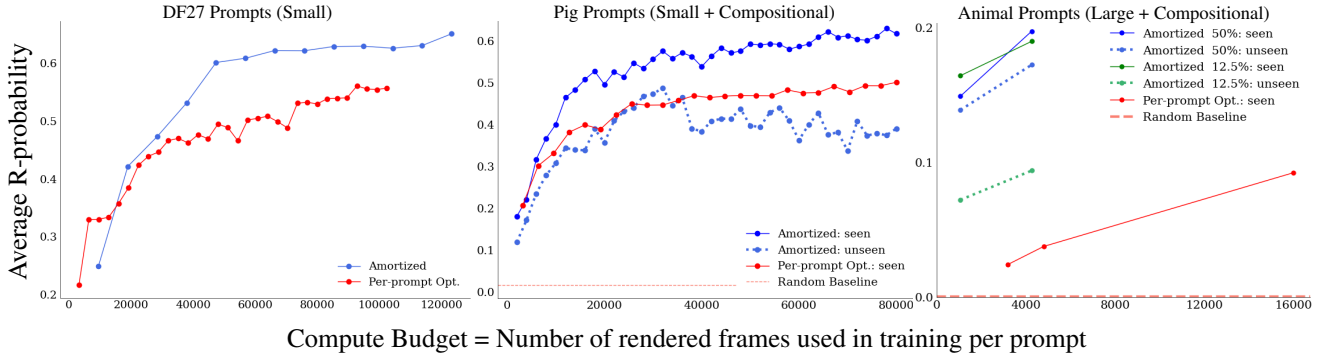


Figure 6: We display the quality against compute budget for a split of **seen** & **unseen** (dashed) prompts with our method (in **blue** and **green**) & existing work’s **per-prompt optimization** baseline (in **red**). Our method is only trained on the seen split of the prompts. At a given training iteration, the amortized model is evaluated zero-shot on unseen prompts. **Takeaway:** For any compute budget, we achieve a higher quality on both the seen and unseen prompts. Our benefits grow for larger, compositional prompt sets. *Left:* The 27 prompts from DreamFusion (Fig. 11). *Middle:* The 64 compositional pig prompts (Fig. 2). **Per-prompt optimization** cannot perform zero-shot generation for unseen prompts, so we report the performance of a random initialization baseline. *Right:* The 2400 compositional animal prompts (Fig. 8), with varying prompt proportions used in training. The generalization gap is small when training on 50% of the prompts. Notably, the cheap testing performance is better than the expensive **per-prompt** method with only 12.5% of the prompts.

Quality: *CLIP R-(prec.)ision* is a text-to-3D correspondence metric introduced in Dream Fields [27], defined as the CLIP model’s accuracy at classifying the correct text input of a rendered image from amongst a set of distractor prompts (i.e., the *query set*). *CLIP R-(prob.)ability* is the probability assigned to the correct prompt instead of the binary accuracy, preserving information about confidence, and reducing noise. We found that R- metrics track each other (App. Fig. 12), so we focus on R-prob. We evaluate R-prob. averaged over the input prompt dataset and four distinct rendered views as in DreamFusion [1], using the entire dataset as our query set. The queries in DF27 are highly dissimilar, so we make the metric harder by adding the DF411 prompts to the query set.

4.2. Can We Reduce Training Cost?

Before evaluating generalization, we see if our method can optimize a diverse prompt collection faster than optimizing individually. Fig. 6 gives the R-probability against compute budget for our method & per-prompt optimization, showing we achieved higher quality for any budget. App. Figs. 11 and 14, qualitatively show we accurately memorize all prompts in DreamFusion’s main paper and extended prompt set for a reduced cost – perhaps from component reuse as in App. Fig. 15. So, we have a powerful optimization method that quickly memorizes training data.

But does the performance generalize to unseen prompts? Current TT3D methods optimize 1 prompt, so any generalization is a valuable contribution. App. Fig. 16 shows unseen composed and interpolated prompts, with promising results, which we improve in Secs. 4.3 and 4.4 respectively.

4.3. Can We Generalize to Unseen Prompts?

Next, we investigate generalizing to unseen prompts with no extra optimization. We used compositional prompt datasets to evaluate (compositional) generalization in the smaller pig and larger animal prompt datasets. Fig. 6 shows R-probability against compute budget on both seen & unseen prompts for our method & per-prompt optimization showing that we achieved higher quality for any compute budget on both prompt sets. Our generalization is especially evident in the larger prompt set, where we held out a significant fraction of the training prompts. With 50% of prompts withheld, we have a minimal generalization gap. With only 12.5% (300) prompts seen during training, generalization to *unseen prompts* was better than per-prompt optimization on *seen prompts* with only $1/4$ the per-prompt compute budget.

To understand the superior performance, we visually compare a subset of pig prompts with the “*holding a blue balloon*” activity in Fig. 7. ATT3D produced more consistent results than per-prompt optimization, potentially explaining our higher R-probability. Visualizations for the pig and animal experiments are in Figs. 2 and 8, respectively. This confirms we can achieve strong generalization performance with a sufficient prompt set. Further, quality can be improved with fine-tuning strategies (App. Fig. 17).

4.4. Can We Make Useful Interpolations?

Next, we investigate our method’s ability to create objects as we interpolate between text prompts with no additional test-time optimization. In Fig. 3, we show rendered outputs as we interpolate between different prompts. The output remains realistic with smooth transitions.

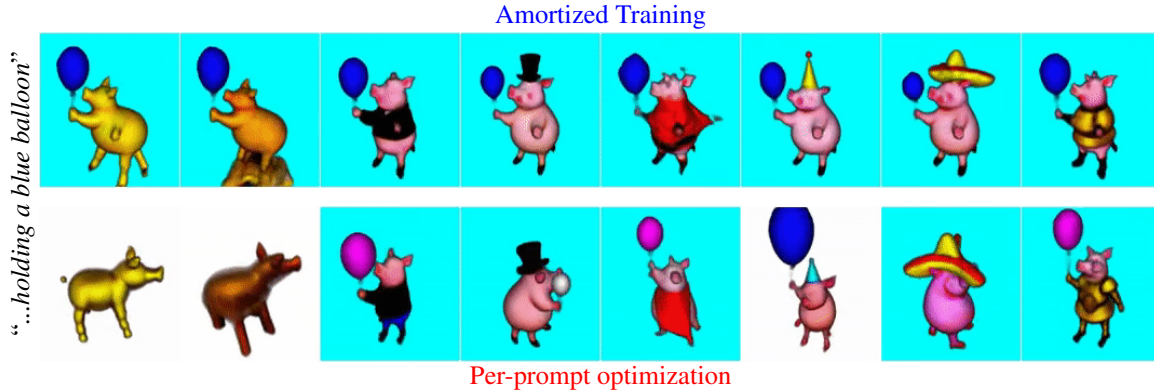


Figure 7: We compare **amortized** and **per-prompt** optimization on the prompts of the form “...*holding a blue balloon*.” Amortization discovers a canonical orientation and always makes the balloon blue, while per-prompt training may only make the background blue or fail altogether, potentially explaining performance improvements in Fig. 6.

For Fig. 3, top right, we *did not* use loss amortization and generalize to interpolants while only training on the 3 rock prompts. But, some prompts gave suboptimal results without interpolant training (App. Fig. 16) which we improved by interpolant amortization (Sec. 3.2.2). We evaluated several prompt interpolation approaches. App. Fig. 18 compares 3 interpolant amortization types: loss weightings, interpolated embeddings, and guidance weightings, showing various ways to control results. App. Fig. 19 compares different interpolant sampling strategies during training, providing qualitatively different ways to generate assets.

5. Related Work

We cover the various fields our method combines: (a) text-to-image generation, then (b) image-to-3D models, which lead to (c) text-to-3D models, which we augment with (d) amortized optimization.

Text-to-image Generation: (A)TT3D methods [1, 2, 15] use large-scale text-conditional DDMs [3, 4, 28–30], which train using classifier-free guidance to sample images matching text prompts [12]. While these models generate diverse and high-fidelity images for many prompts, they cannot provide view-consistent renderings of a single object and are thus incapable of making 3D assets directly.

Image-to-3D Models: Beyond using 3D assets to train 3D generative models, prior work has also used image datasets. Most of these methods use NeRFs [6, 17, 31–34] as a differentiable renderer optimized to produce image datasets. Differentiable mesh rendering is an alternative [35–38]. Chan et al. [9] are closely related in this category, using a StyleGAN generator modulated with a learned latent code to produce a triplanar grid that is spatially interpolated and fed through a NeRF producing a static image dataset. We also modulate spatially oriented feature grids, without relying on memory-intensive pre-trained generator backbones. These techniques may prove valuable in future work scaling to ultra-large prompt sets.

Text-to-3D Generation: Recent advances include CLIP-forge [39], CLIP-mesh [40], Latent-NeRF [41], Dream Field [27], Score-Jacobian-Chaining [15], & DreamFusion [1]. In CLIP-forge [39], the model is trained for shapes conditioned on CLIP text embeddings from rendered images. During inference, the embedding is provided for the generative model to synthesize new shapes based on the text. CLIP-mesh [40] and Dream Field [27] optimized the underlying 3D representation with the CLIP-based loss. Magic3D adds a finetuning phase with a textured-mesh model [42], allowing high resolutions. Future advances may arise by combining with techniques from unconditional 3D generation [43–45]. Notable open-source contributions are Stable-Dreamfusion [46] and threestudio [47]. Other concurrent works include Zero-1-to-3 [48], Fantasia3D [49], Dream3D [50], DreamAvatar [51], and Prolific-Dreamer [52]. However, we differ from all of these text-to-3D works, because we amortize over the text prompts.

Amortized Optimization: Amortized optimization [16] is a tool of blossoming importance in learning to optimize [53] and machine learning, with applications to meta-learning [54], hyperparameter optimization [55, 56], and generative modeling [26, 57–59]. Hypernetworks [60] are a popular tool for amortization [55, 56, 61, 62] and have also been used to modulate NeRFs [17, 63, 64], inspiring our strategy. Our method differs from prior works by modulating spatially oriented parameters, and our objective is from a (dynamic) DDM instead of a (static) dataset.

Text-to-3D Animation: Text-to-4D [65] is an approach for directly making 3D animations from text, instead of our interpolation strategy. This is done by generalizing TT3D to use a text-to-video model [28, 66, 67], instead of a text-to-image model. However, unlike us, this requires text-to-video, which can require video data.

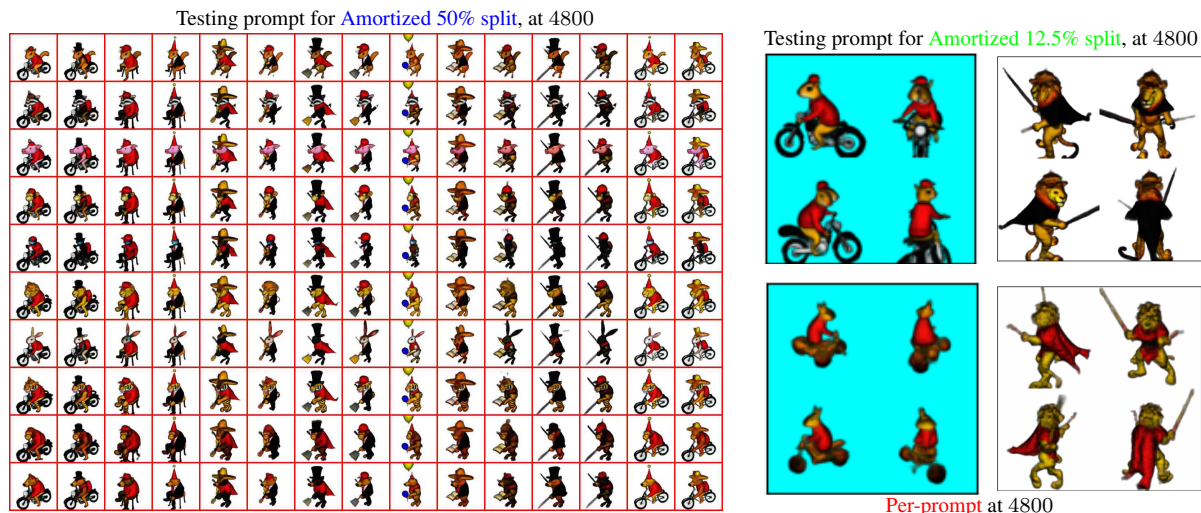


Figure 8: We show quantitative results for the 2400 animal prompts in Fig. 6, where we achieve a higher quality for any compute budget on seen & unseen prompts. Notably, when training on only 50% or 12.5% of the prompts, the unseen prompts – which cost no optimization – perform stronger than the **per-prompt** method, which must optimize on the data. **Takeaway:** By training a single model on many text prompts we generalize to unseen prompts without extra optimization.

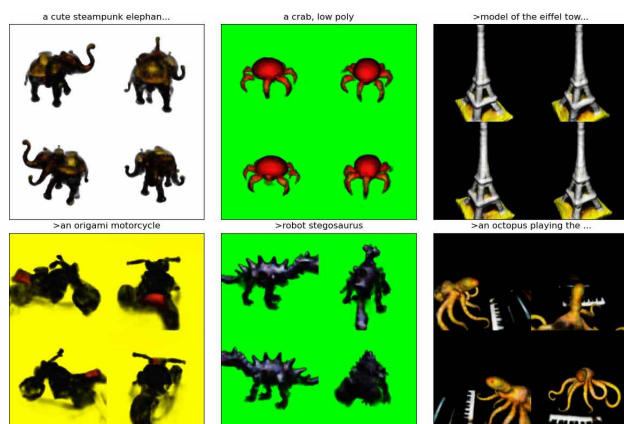


Figure 9: Results for amortized training on DreamFusion’s extended set of 411 text prompts, DF411. See Fig. 14 for the full set. **Takeaway:** We scale to diverse prompt sets $>10\times$ larger than DF27 (Fig. 11) with minor quality drop.

6. Conclusion

We presented ATT3D, a method for amortized optimization of text-to-3D (TT3D) models. We use a mapping network from text to NeRFs, enabling a single model to represent 3D objects of many different prompts. We experimentally validate our method on existing and new compositional prompt sets. We are faster at training than current TT3D methods by sharing the optimization cost across a prompt set. Once trained, our model generalizes by directly outputting objects for prompts unseen during training in a single forward pass. Furthermore, by amortizing over interpolation weights, we quickly generate a continuum of interpolations between prompts, enhancing user control.

Although ATT3D only represents a small step towards general and fast text-to-3D generation, we believe that the ideas presented are a promising avenue toward this future.

Limitations: Our method builds on the existing text-to-3D optimization paradigm, so we share several limitations with these works: More powerful text-to-image DDMs may be required for higher quality and robustness in results. The objective has high variance, and the system can be sensitive to prompt engineering. We also suffer from a lack of diversity, as in prior work. We found that similar prompts can collapse to the same scene when amortizing. Finally, larger object-centric prompt sets are required to further test the scaling of amortized training.

Ethics Statement: Text-to-image models carry ethical concerns for synthesizing images, which text-to-3D models like this share. For example, we may inherit any biases in our underlying text-to-image model. These models could displace creative jobs or enable the growth and accessibility of 3D asset generation. Alternatively, 3D synthesis models could be used to generate misinformation by bad actors.

Reproducibility Statement: Our instant-NGP NeRF backbone is publicly available through the “instant-ngp” repository [7]. While our diffusion model is not publicly available (as in DreamFusion [1]), other available models may be used to produce similar results. To aid reproducibility, we include a method schematic in Fig. 4 and pseudocode in Alg. 1. Our evaluation setup is in Sec. 4.1 along with hyperparameters and other details in App. Sec. B.

Acknowledgements

We thank Weiwei Sun, Matan Atzmon, and Or Perel for helpful feedback. The Python community [68, 69] made underlying tools, including PyTorch [70] & Matplotlib [71].

Disclosure of Funding

NVIDIA funded this work. Jonathan Lorraine, Kevin Xie, Xiaohui Zeng, and Towaki Takikawa had funding from student scholarships at the University of Toronto and the Vector Institute, which are not in direct support of this work.

References

- [1] Ben Poole, Ajay Jain, Jonathan T Barron, and Ben Mildenhall. Dreamfusion: Text-to-3d using 2d diffusion. *arXiv:2209.14988*, 2022. 1, 2, 3, 4, 6, 7, 8, 12, 13, 14, 16
- [2] Chen-Hsuan Lin, Jun Gao, Luming Tang, Towaki Takikawa, Xiaohui Zeng, Xun Huang, Karsten Kreis, Sanja Fidler, Ming-Yu Liu, and Tsung-Yi Lin. Magic3d: High-resolution text-to-3d content creation. *arXiv:2211.10440*, 2022. 1, 7, 12, 14, 19, 20
- [3] Yogesh Balaji, Seungjun Nah, Xun Huang, Arash Vahdat, Jiaming Song, Karsten Kreis, Miika Aittala, Timo Aila, Samuli Laine, Bryan Catanzaro, et al. ediffi: Text-to-image diffusion models with an ensemble of expert denoisers. *arXiv:2211.01324*, 2022. 1, 3, 7
- [4] Robin Rombach, Andreas Blattmann, Dominik Lorenz, Patrick Esser, and Björn Ommer. High-resolution image synthesis with latent diffusion models. In *IEEE/CVF Conference on Computer Vision and Pattern Recognition*, 2022. 7
- [5] Chitwan Saharia, William Chan, Saurabh Saxena, Lala Li, Jay Whang, Emily Denton, Seyed Kamyar Seyed Ghasemipour, Burcu Karagol Ayan, S Sara Mahdavi, Rapha Gontijo Lopes, et al. Photorealistic text-to-image diffusion models with deep language understanding. *arXiv:2205.11487*, 2022. 1, 3
- [6] Ben Mildenhall, Pratul P Srinivasan, Matthew Tancik, Jonathan T Barron, Ravi Ramamoorthi, and Ren Ng. Nerf: Representing scenes as neural radiance fields for view synthesis. *Communications of the ACM*, 2021. 3, 7, 12
- [7] Thomas Müller, Alex Evans, Christoph Schied, and Alexander Keller. Instant neural graphics primitives with a multiresolution hash encoding. *arXiv:2201.05989*, 2022. 3, 8, 12
- [8] Towaki Takikawa, Alex Evans, Jonathan Tremblay, Thomas Müller, Morgan McGuire, Alec Jacobson, and Sanja Fidler. Variable bitrate neural fields. In *ACM SIGGRAPH 2022 Conference Proceedings*, 2022.
- [9] Eric R Chan, Connor Z Lin, Matthew A Chan, Koki Nagano, Boxiao Pan, Shalini De Mello, Orazio Gallo, Leonidas J Guibas, Jonathan Tremblay, Sameh Khamis, et al. Efficient geometry-aware 3d generative adversarial networks. In *IEEE/CVF Conference on Computer Vision and Pattern Recognition*, 2022. 3, 7
- [10] Jonathan Ho, Ajay Jain, and Pieter Abbeel. Denoising diffusion probabilistic models. *Advances in Neural Information Processing Systems*, 2020. 3
- [11] Yang Song, Jascha Sohl-Dickstein, Diederik P Kingma, Abhishek Kumar, Stefano Ermon, and Ben Poole. Score-based generative modeling through stochastic differential equations. *arXiv:2011.13456*, 2020. 3
- [12] Jonathan Ho and Tim Salimans. Classifier-free diffusion guidance. *arXiv:2207.12598*, 2022. 3, 7
- [13] Colin Raffel, Noam Shazeer, Adam Roberts, Katherine Lee, Sharan Narang, Michael Matena, Yanqi Zhou, Wei Li, and Peter J. Liu. Exploring the limits of transfer learning with a unified text-to-text transformer. *JMLR*, 2020. 3
- [14] Alec Radford, Jong Wook Kim, Chris Hallacy, Aditya Ramesh, Gabriel Goh, Sandhini Agarwal, Girish Sastry, Amanda Askell, Pamela Mishkin, Jack Clark, Gretchen Krueger, and Ilya Sutskever. Learning transferable visual models from natural language supervision. 2021. 3
- [15] Haochen Wang, Xiaodan Du, Jiahao Li, Raymond A Yeh, and Greg Shakhnarovich. Score jacobian chaining: Lifting pretrained 2d diffusion models for 3d generation. *arXiv:2212.00774*, 2022. 3, 7
- [16] Brandon Amos. Tutorial on amortized optimization for learning to optimize over continuous domains. *arXiv:2202.00665*, 2022. 3, 7
- [17] Daniel Rebaïn, Mark J Matthews, Kwang Moo Yi, Gopal Sharma, Dmitry Lagun, and Andrea Tagliasacchi. Attention beats concatenation for conditioning neural fields. *arXiv:2209.10684*, 2022. 3, 7, 12
- [18] Ian Goodfellow, Jean Pouget-Abadie, Mehdi Mirza, Bing Xu, David Warde-Farley, Sherjil Ozair, Aaron Courville, and Yoshua Bengio. Generative adversarial networks. *Communications of the ACM*, 2020. 4, 5
- [19] Takeru Miyato, Toshiki Kataoka, Masanori Koyama, and Yuichi Yoshida. Spectral normalization for generative adversarial networks. *arXiv:1802.05957*, 2018. 4
- [20] Andrew Brock, Jeff Donahue, and Karen Simonyan. Large scale gan training for high fidelity natural image synthesis. *arXiv:1809.11096*, 2018. 4
- [21] David Pfau and Oriol Vinyals. Connecting generative adversarial networks and actor-critic methods. *arXiv:1610.01945*, 2016. 4
- [22] Gauthier Gidel, Reyhane Askari Hemmat, Mohammad Pezeshki, Rémi Le Priol, Gabriel Huang, Simon Lacoste-Julien, and Ioannis Mitliagkas. Negative momentum for improved game dynamics. In *The 22nd International Conference on Artificial Intelligence and Statistics*, 2019. 4

- [23] Jonathan P Lorraine, David Acuna, Paul Vicol, and David Duvenaud. Complex momentum for optimization in games. In *International Conference on Artificial Intelligence and Statistics*, pages 7742–7765. PMLR, 2022. 4
- [24] Rohan Anil, Vineet Gupta, Tomer Koren, Kevin Regan, and Yoram Singer. Scalable second order optimization for deep learning. *arXiv:2002.09018*, 2020. 4
- [25] Diederik P Kingma and Jimmy Ba. Adam: A method for stochastic optimization. *arXiv:1412.6980*, 2014. 4
- [26] Diederik P Kingma and Max Welling. Auto-encoding variational bayes. *arXiv:1312.6114*, 2013. 5, 7, 12
- [27] Ajay Jain, Ben Mildenhall, Jonathan T Barron, Pieter Abbeel, and Ben Poole. Zero-shot text-guided object generation with dream fields. In *CVF Conference on Computer Vision and Pattern Recognition Proceedings*, 2022. 6, 7
- [28] Jonathan Ho, William Chan, Chitwan Saharia, Jay Whang, Ruiqi Gao, Alexey Gritsenko, Diederik P Kingma, Ben Poole, Mohammad Norouzi, David J Fleet, et al. Imagen video: High definition video generation with diffusion models. *arXiv:2210.02303*, 2022. 7
- [29] Aditya Ramesh, Prafulla Dhariwal, Alex Nichol, Casey Chu, and Mark Chen. Hierarchical text-conditional image generation with clip latents. *arXiv:2204.06125*, 2022.
- [30] Alex Shonenkov, Misha Konstantinov, Daria Bakshandaeva, Christoph Schuhmann, Ksenia Ivanova, and Nadiia Klokova. If by deepfloyd lab at stabilityai, 2023. github.com/deep-floyd/IF. 7
- [31] Daniel Rebain, Mark Matthews, Kwang Moo Yi, Dmitry Lagun, and Andrea Tagliasacchi. Lolerf: Learn from one look. In *IEEE/CVF Conference on Computer Vision and Pattern Recognition*, 2022. 7
- [32] Eric R Chan, Marco Monteiro, Petr Kellnhofer, Jiajun Wu, and Gordon Wetzstein. pi-gan: Periodic implicit generative adversarial networks for 3d-aware image synthesis. In *IEEE/CVF conference on computer vision and pattern recognition*, 2021.
- [33] Luke Melas-Kyriazi, Iro Laina, Christian Rupprecht, and Andrea Vedaldi. Realfusion: 360deg reconstruction of any object from a single image. In *IEEE/CVF Conference on Computer Vision and Pattern Recognition*, 2023.
- [34] Junshu Tang, Tengfei Wang, Bo Zhang, Ting Zhang, Ran Yi, Lizhuang Ma, and Dong Chen. Make-it-3d: High-fidelity 3d creation from a single image with diffusion prior. *arXiv:2303.14184*, 2023. 7
- [35] Dario Pavlo, Jonas Kohler, Thomas Hofmann, and Aurelien Lucchi. Learning generative models of textured 3d meshes from real-world images. In *IEEE/CVF International Conference on Computer Vision*, 2021. 7
- [36] Jun Gao, Tianchang Shen, Zian Wang, Wenzheng Chen, Kangxue Yin, Daiqing Li, Or Litany, Zan Gojcic, and Sanja Fidler. Get3d: A generative model of high quality 3d textured shapes learned from images. *arXiv:2209.11163*, 2022.
- [37] Dario Pavlo, Graham Spinks, Thomas Hofmann, Marie-Francine Moens, and Aurelien Lucchi. Convolutional generation of textured 3d meshes. *Advances in Neural Information Processing Systems*, 2020.
- [38] Wenzheng Chen, Huan Ling, Jun Gao, Edward Smith, Jaakko Lehtinen, Alec Jacobson, and Sanja Fidler. Learning to predict 3d objects with an interpolation-based differentiable renderer. *Advances in Neural Information Processing Systems*, 32, 2019. 7
- [39] Aditya Sanghi, Hang Chu, Joseph Lambourne, Ye Wang, Chin-Yi Cheng, and Marco Fumero. Clip-forge: Towards zero-shot text-to-shape generation. *arXiv:2110.02624*, 2021. 7
- [40] Nasir Khalid, Tianhao Xie, Eugene Belilovsky, and Tiberiu Popa. Clip-mesh: Generating textured meshes from text using pretrained image-text models. *ACM Transactions on Graphics (TOG), Proc. SIGGRAPH Asia*, 2022. 7
- [41] Gal Metzer, Elad Richardson, Or Patashnik, Raja Giryes, and Daniel Cohen-Or. Latent-nerf for shape-guided generation of 3d shapes and textures. In *IEEE/CVF Conference on Computer Vision and Pattern Recognition*, 2023. 7
- [42] Tianchang Shen, Jun Gao, Kangxue Yin, Ming-Yu Liu, and Sanja Fidler. Deep marching tetrahedra: a hybrid representation for high-resolution 3d shape synthesis. *Advances in Neural Information Processing Systems*, 2021. 7
- [43] Miguel Angel Bautista, Pengsheng Guo, Samira Abnar, Walter Talbott, Alexander Toshev, Zhuoyuan Chen, Laurent Dinh, Shuangfei Zhai, Hanlin Goh, Daniel Ulbricht, et al. Gaudi: A neural architect for immersive 3d scene generation. *arXiv:2207.13751*, 2022. 7
- [44] Xiaohui Zeng, Arash Vahdat, Francis Williams, Zan Gojcic, Or Litany, Sanja Fidler, and Karsten Kreis. Lion: Latent point diffusion models for 3d shape generation. In *Advances in Neural Information Processing Systems (NeurIPS)*, 2022.
- [45] Linqi Zhou, Yilun Du, and Jiajun Wu. 3d shape generation and completion through point-voxel diffusion. In *IEEE/CVF International Conference on Computer Vision*, 2021. 7
- [46] Jiayang Tang. Stable-dreamfusion: Text-to-3d with stable-diffusion, 2022. github.com/ashawkey/stable-dreamfusion. 7
- [47] Yuan-Chen Guo, Ying-Tian Liu, Chen Wang, Zi-Xin Zou, Guan Luo, Chia-Hao Chen, Yan-Pei Cao, and Song-Hai Zhang. threestudio: A unified framework for 3d content generation. github.com/threestudio-project/threestudio, 2023. 7

- [48] Ruoshi Liu, Rundi Wu, Basile Van Hoorick, Pavel Tokmakov, Sergey Zakharov, and Carl Vondrick. Zero-1-to-3: Zero-shot one image to 3d object. *arXiv:2303.11328*, 2023. 7
- [49] Rui Chen, Yongwei Chen, Ningxin Jiao, and Kui Jia. Fantasia3d: Disentangling geometry and appearance for high-quality text-to-3d content creation. *arXiv:2303.13873*, 2023. 7
- [50] Jiale Xu, Xintao Wang, Weihao Cheng, Yan-Pei Cao, Ying Shan, Xiaohu Qie, and Shenghua Gao. Dream3d: Zero-shot text-to-3d synthesis using 3d shape prior and text-to-image diffusion models. In *IEEE/CVF Conference on Computer Vision and Pattern Recognition*, 2023. 7
- [51] Yukang Cao, Yan-Pei Cao, Kai Han, Ying Shan, and Kwan-Yee K Wong. Dreamavatar: Text-and-shape guided 3d human avatar generation via diffusion models. *arXiv:2304.00916*, 2023. 7
- [52] Zhengyi Wang, Cheng Lu, Yikai Wang, Fan Bao, Chongxuan Li, Hang Su, and Jun Zhu. Prolificdreamer: High-fidelity and diverse text-to-3d generation with variational score distillation. *arXiv:2305.16213*, 2023. 7
- [53] Tianlong Chen, Xiaohan Chen, Wuyang Chen, Howard Heaton, Jialin Liu, Zhangyang Wang, and Wotao Yin. Learning to optimize: A primer and a benchmark. *arXiv:2103.12828*, 2021. 7
- [54] Timothy Hospedales, Antreas Antoniou, Paul Micaelli, and Amos Storkey. Meta-learning in neural networks: A survey. *IEEE transactions on pattern analysis and machine intelligence*, 2021. 7
- [55] Jonathan Lorraine and David Duvenaud. Stochastic hyperparameter optimization through hypernetworks. *arXiv:1802.09419*, 2018. 7
- [56] Matthew Mackay, Paul Vicol, Jonathan Lorraine, David Duvenaud, and Roger Grosse. Self-tuning networks: Bilevel optimization of hyperparameters using structured best-response functions. In *International Conference on Learning Representations*, 2018. 7
- [57] Danilo Jimenez Rezende, Shakir Mohamed, and Daan Wierstra. Stochastic backpropagation and approximate inference in deep generative models. In *ICML*, 2014. 7
- [58] Chris Cremer, Xuechen Li, and David Duvenaud. Inference suboptimality in variational autoencoders. In *International Conference on Machine Learning*, 2018.
- [59] Mike Wu, Kristy Choi, Noah Goodman, and Stefano Ermon. Meta-amortized variational inference and learning. In *AAAI Conference on Artificial Intelligence*, 2020. 7
- [60] David Ha, Andrew Dai, and Quoc V Le. Hypernetworks. *arXiv:1609.09106*, 2016. 7
- [61] Chris Zhang, Mengye Ren, and Raquel Urtasun. Graph hypernetworks for neural architecture search. *arXiv:1810.05749*, 2018. 7
- [62] Boris Knyazev, Michal Drozdal, Graham W Taylor, and Adriana Romero Soriano. Parameter prediction for unseen deep architectures. *Advances in Neural Information Processing Systems*, 2021. 7
- [63] Vincent Sitzmann, Eric Chan, Richard Tucker, Noah Snavely, and Gordon Wetzstein. Metasdf: Meta-learning signed distance functions. *Advances in Neural Information Processing Systems*, 2020. 7
- [64] Emilien Dupont, Hyunjik Kim, SM Ali Eslami, Danilo Jimenez Rezende, and Dan Rosenbaum. From data to functa: Your data point is a function and you can treat it like one. In *ICML*, 2022. 7
- [65] Uriel Singer, Shelly Sheynin, Adam Polyak, Oron Ashual, Iurii Makarov, Filippos Kokkinos, Naman Goyal, Andrea Vedaldi, Devi Parikh, Justin Johnson, et al. Text-to-4d dynamic scene generation. *arXiv:2301.11280*, 2023. 7
- [66] Uriel Singer, Adam Polyak, Thomas Hayes, Xi Yin, Jie An, Songyang Zhang, Qiyuan Hu, Harry Yang, Oron Ashual, Oran Gafni, et al. Make-a-video: Text-to-video generation without text-video data. *arXiv:2209.14792*, 2022. 7
- [67] Andreas Blattmann, Robin Rombach, Huan Ling, Tim Dockhorn, Seung Wook Kim, Sanja Fidler, and Karsten Kreis. Align your latents: High-resolution video synthesis with latent diffusion models. In *IEEE/CVF Conference on Computer Vision and Pattern Recognition*, 2023. 7
- [68] Guido Van Rossum and Fred L Drake Jr. *Python reference manual*. Centrum voor Wiskunde en Informatica Amsterdam, 1995. 9
- [69] Travis E Oliphant. Python for scientific computing. *Computing in Science & Engineering*, 2007. 9
- [70] Adam Paszke, Sam Gross, Soumith Chintala, Gregory Chanan, Edward Yang, Zachary DeVito, Zeming Lin, Alban Desmaison, Luca Antiga, and Adam Lerer. Automatic differentiation in PyTorch. *Openreview*, 2017. 9, 15
- [71] John D Hunter. Matplotlib: A 2D graphics environment. *Computing in Science & Engineering*, 2007. 9
- [72] Dan Hendrycks and Kevin Gimpel. Gaussian error linear units (gelus). *arXiv:1606.08415*, 2016. 12
- [73] Ashish Vaswani, Noam Shazeer, Niki Parmar, Jakob Uszkoreit, Llion Jones, Aidan N Gomez, Łukasz Kaiser, and Illia Polosukhin. Attention is all you need. *Advances in neural information processing systems*, 2017. 13
- [74] Dor Verbin, Peter Hedman, Ben Mildenhall, Todd Zickler, Jonathan T Barron, and Pratul P Srinivasan. Ref-nerf: structured view-dependent appearance for neural radiance fields. In *IEEE/CVF Conference on Computer Vision and Pattern Recognition (CVPR)*, 2022. 13

Table 1: Glossary and notation

(A)TT3D	(Amortized) Text-to-3D
NeRF	Neural Radiance Field [6]
DDM	Denosing Diffusion Model
MLP	Multi-layer Perceptron
DF27, DF411	DreamFusion’s [1] 27 main text prompts & the extended 411 prompts
$n, m \in \mathbb{N}$	The size of different objects
$x, y, z, \dots \in \mathbb{R}$	Scalar coordinates
$\mathbf{x}, \mathbf{y}, \mathbf{z}, \dots \in \mathbb{R}^n$	Vectors
$\mathcal{X}, \mathcal{Y}, \mathcal{Z}, \dots$	The domain of $\mathbf{x}, \mathbf{y}, \mathbf{z}, \dots$
$\mathbf{x} = [x, y, z] \in \mathcal{X}$	A point
$\mathbf{r} = [\sigma, r, g, b] \in \mathcal{R}$	The density and color values
$\mathbf{w} \in \mathcal{W}$	The parameters of the point encoder function
$\gamma_{\mathbf{w}} : \mathcal{X} \rightarrow \Gamma$	The point encoder function
$\nu : \Gamma \rightarrow \mathcal{R}$	The final MLP mapping point encodings to radiance
\mathbf{z}	The problem context for amortization
$\mathbf{c} \in \mathcal{C}$	A text embedding used to condition the DDM and as problem context
$\mathbf{m} : \mathcal{C} \rightarrow \mathcal{W}$	The mapping network from problem context to modulations
$\mathbf{v} \in \mathbb{R}^n$	The intermediary vector-embedding of \mathbf{c} in \mathbf{m}
$\mathcal{N}, \mathcal{U}, \text{Dir}, \text{Bern}$	Normal, uniform, Dirichlet, and Bernoulli distributions respectively
$\epsilon, \hat{\epsilon}$	Noise added to rendered frames, or as predicted by the DDM
$\kappa \in \mathbb{R}^+$	The concentration parameter of the Dirichlet distribution
$\alpha \in [0, 1]$	An interpolation coefficient, sampled from $\text{Dir}(\kappa)$ in training
\mathcal{L}	A loss function
ω	A guidance weight
β_1, β_2	Parameters of the Adam optimizer [26]

A. Glossary

B. Experimental Setup

B.1. Implementation Details

We replicate DreamFusion [1] and Magic3D’s [2] setup where possible and list key details here. We recommend reading these papers for additional context.

B.1.1 Point-encoder γ

We followed Instant NGP [7] to parameterize our NeRF, consisting of dense, multi-resolution voxel grids and dictionaries. We only use dense voxel layers unless specified, which trained faster with negligible quality drop. For our multi-resolution voxel grid, we use resolutions of [9, 14, 22, 36, 58], with 4 features per level. When active, we use a further three levels of hash grid parameters. Each level’s features are linearly interpolated according to spatial location and concatenated, leading to a final output feature size of 20 with dense voxel grids and 32 with the full INGP.

B.1.2 Final NeRF MLP ν

We select a minimal final MLP to maintain evaluation speed, with a single hidden layer with 32 units and a SiLU activation [72]. The majority of our model’s capacity comes from the point-encoder. We use a softplus activation for the density output and sigmoid activations on the color.

B.1.3 Mapping Network \mathbf{m}

The mapping network computes a fixed-size vector representation \mathbf{v} of the task from the text embedding. We only use the CLIP embedding for feature grid modulation because it was sufficient and including the T5 embedding increases network size. We apply spectral normalization to all linear layers. We considered concatenation, hypernetwork, and attention approaches for modulation [17]:

Concatenation: The simple strategy of naïvely concatenating (a vector-representation f of) the text to the point-encoding – i.e., $\nu(\gamma_{\mathbf{w}}(\mathbf{x}), f(\mathbf{c}))$ was prohibitively expensive. This is because we require the cost of the final per-point NeRF MLP ν to be minimal for cheap rendering. The concatenation approach of $\nu(\gamma_{\mathbf{w}}(\mathbf{x}), \mathbf{v})$ introduces overhead by increasing per-iteration training time by 37% but doesn’t significantly impact quality. In inference, the hypernet method is superior, reducing cost by $\sim 20 - 75\%$, as we only generate the grid parameters \mathbf{w} once when rendering multiple views of 1 object, bypassing the use of a single, larger NeRF ν with concatenation.

Hypernetwork: We first flatten the token and pass it through an MLP to produce a vector-embedding, which is used by a linear layer to output the point-encoder’s voxel grid parameters. As the CLIP embedding was already a strong representation, we found that a simple linear layer for the text-embedding to vector-embedding was sufficient.

We converged with deeper hypernetworks – by using spectral normalization on all linear layers – but this offered no quality benefit while taking longer to train. We also found removing the bias on the final linear layer decreased noise by forcing the result to depend on the prompt.

We vary the vector embedding v 's size in our experiments, which largely dictates our amortized model's capacity. The mapping network m dominates the model's memory cost, while the text's vector-embedding largely dictates the mapping network size. Our memory cost scales linearly with the vector-embedding size. We use a vector embedding v size of 32 for all experiments except interpolation, where we use 2. We have experiments where the number of text prompts is both smaller (DF27) and larger (DF411, compositional prompts) than the vector-embedding.

Attention: We also investigated using an attention-based mapping network with a series of self-attention layers to process text embeddings before feeding into the hypernetworks for each multi-resolution grid level. Our attention performed with comparable quality but trained more slowly. However, we expect modifications to be necessary on more complex prompt sets.

B.1.4 Environment Mapping Network

In our experiments, we use a background, a function mapping ray directions – and text embeddings – to colors, which we denote as the environment map. Specifically, we encode the ray directions, concatenate them with the vector-embedding v from the mapping network, and feed them into a final MLP. We use a sigmoid activation on the output color and spectral norm on all linear layers. We encode the ray directions with a sinusoidal positional encoding [73] (frequencies $2^0, 2^1, \dots, 2^{L-1}$, $L = 8$), and no hidden layers — i.e., a linear layer — for our final MLP.

B.1.5 Spectral Normalization

We found spectral normalization – which can be implemented trivially in PyTorch on linear layers – to be critical for mapping net training, but non-essential on other parts. In the mapping network, we must use spectral normalization on all linear layers for the hypernetwork and attention approaches or we suffer from numerical instability. Using spectral normalization on the linear layers in the environment map, or final NeRF module was unnecessary.

B.1.6 Sampling Text Prompts

We cache the CLIP (and T5) embeddings for all experiments to avoid repeated computation and the memory overhead of the large text encoders. We use multiple text prompts in each batched update.

Interpolations: We sample interpolated embeddings during training in interpolation experiments (Section 4.4). See Section B.1.14 or Figure 18 for more interpolation setup details. When interpolating between prompts with text-embeddings c_1 and c_2 , we sample a weight $\alpha \in [0, 1]$ and input $c' = (1 - \alpha)c_1 + \alpha c_2$ to the mapping network.

B.1.7 Sampling Rendering Conditions

As in DreamFusion [1], we randomly sample rendering conditions, including the camera position and lighting conditions. We use a bounding sphere of radius 2 in all experiments. We sample the point light location with distance from $\mathcal{U}(1, 3)$ and angle relative to the random camera position of $\mathcal{U}(0, \pi/4)$. We sample “soft” textureless and albedo-only augmentations to allow varying shades during training. Also, we sample the camera distance from $\mathcal{U}(2, 3)$ and the focal length from $\mathcal{U}(0.7, 1.35)$.

B.1.8 Score Distillation Sampling

For the DDM's sampling, we sample the time-step from $\mathcal{U}(0.002, 1.0)$ and use a guidance weight of 100.

B.1.9 The Objective

The regularizers: The orientation loss [74] (as in DreamFusion [1]) encourages normal vectors of the density field to face the camera when visible, preventing the model from changing colors to be darker during textureless renders by making geometry face “backward” when shaded. Also, DreamFusion regularizes accumulated alpha value along each ray, encouraging not unnecessarily filling space and aiding in foreground/background separation. We do not use these regularizers for all experiments, as we did not observe failure modes they fixed, and they made no significant change in results over the interval $[10^{-3}, 10^{-1}]$. Larger opacity regularization values resulted in empty scenes, while larger orientation values did not change the initialization from a sphere.

The image fidelity: We train with 32 points sampled uniformly along each ray for all experiments except interpolations. For interpolations only, we sample 128 points and reduced batch size to improve quality. Our underlying text-to-image model generates 64×64 images, leading to 4096 rays per rendered frame. At inference time we render with higher points per ray to improve quality for negligible cost.

The initialization: As in DreamFusion, we add an initial spatial density bias to prevent collapsing to an empty scene, shown in Figure 10, left. Our density bias on the NeRF MLP output before the softplus activation takes the form:

$$\text{densityBias}(\mathbf{x}) = 10(1 - 2\|\mathbf{x}\|_2) \quad (7)$$

B.1.10 The Optimization

We use Adam with a learning rate of 1×10^{-1} and $\beta_2 = 0.999$. A wide range momentum β_1 (up to .95) can yield similar qualities if the step size is jointly tuned, while the quickest convergence occurs at 0. We do not use the linear learning rate warmup or cosine decay from DreamFusion.

B.1.11 Memorization Experiments

Our experiments use the same architecture for per-prompt and amortized training settings to ensure a fair comparison. We train models using a batch size of 32 times the number of GPUs used. Amortized training uses 8 GPUs while per-prompt uses a single GPU (due to resource constraints), with more details in Section B.2. The complete set of DreamFusion prompts is located here: <https://dreamfusion3d.github.io/gallery.html>

B.1.12 Generalization Experiments

Our prompt selections are motivated by the compositional experiment in DreamFusion’s Figure 4 [1]. Our experiments with pig prompts with the template “*a pig {activity} {theme}*”, where the `activities` and `themes` are any combination of the following:

The activities: [“*riding a bicycle*”, “*sitting on a chair*”, “*playing the guitar*”, “*holding a shovel*”, “*holding a blue balloon*”, “*holding a book*”, “*wielding a katana*”, “*riding a bike*”]

The themes: [“*made out of gold*”, “*carved out of wood*”, “*wearing a leather jacket*”, “*wearing a tophat*”, “*wearing a party hat*”, “*wearing a sombrero*”, “*wearing medieval armor*”]

Our pig holdout, unseen, testing prompts are pairing the i^{th} activity and theme.

Our experiments with animal prompts with the template “*{animal} {activity} {theme} {hat}*”, where the `activities`, `themes` and `hats` are any combination of the following:

The animals: [“*a squirrel*”, “*a raccoon*”, “*a pig*”, “*a monkey*”, “*a robot*”, “*a lion*”, “*a rabbit*”, “*a tiger*”, “*an orangutan*”, “*a bear*”]

The activities: [“*riding a motorcycle*”, “*sitting on a chair*”, “*playing the guitar*”, “*holding a shovel*”, “*holding a blue balloon*”, “*holding a book*”, “*wielding a katana*”]

The themes: [“*wearing a leather jacket*”, “*wearing a sweater*”, “*wearing a cape*”, “*wearing medieval armor*”, “*wearing a backpack*”, “*wearing a suit*”]

The hats: [“*wearing a party hat*”, “*wearing a sombrero*”, “*wearing a helmet*”, “*wearing a tophat*”, “*wearing a backpack*”, “*wearing a baseball cap*”]

Our holdout, unseen, animal testing prompts are selected homogeneously for each training set size.

B.1.13 Finetuning Experiments

We resume training from an amortized training checkpoint while re-initializing the optimizer state. For the finetuning experiments, in our mapping network, we only finetune an offset to the output and detach all prior weights that only embed text tokens (because we finetune with one prompt). Other training details are kept equal to per-prompt training.

B.1.14 Interpolation Experiments

In interpolations we use 128 ray samples and batch size 16.

Interpolant concentration: We sample the interpolation coefficient $\alpha \sim \text{Dir}(\kappa)$ from a Dirichlet distribution with concentration parameter κ . The Dirichlet distribution allows us to smoothly interpolate from sampling the original text tokens (with concentration $\kappa \approx 0$, to uniformly sampling α (with concentration $\kappa \approx 1$) to focusing on difficult midpoints (with concentration $\kappa > 1$) – see Figure 19. Specifically, in Figures 3 & 20 we use $\kappa = 2.0$ for 5000 steps to stabilize the midpoint, followed by $\kappa = 0.5$ to focus on the original prompts.

Interpolation types: We provide multiple examples of interpolation types to amortize over that provide qualitatively different results – see Figure 18.

A simple strategy is to interpolate over the text embedding used to condition the text-to-image model:

$$\mathbf{c}' = (1 - \alpha)\mathbf{c}_1 + \alpha\mathbf{c}_2 \quad (8)$$

Another strategy is to interpolate the loss function used between the two prompts. We could evaluate the loss at both prompts and weight the loss:

$$\mathcal{L}_{\text{final}} = (1 - \alpha)\mathcal{L}_{\text{prompt 1}} + \alpha\mathcal{L}_{\text{prompt 2}} \quad (9)$$

Instead, to interpolate in the loss, we sample the loss for each prompt with probability α , which we equate to training with embedding:

$$\mathbf{c}' = (1 - Z)\mathbf{c}_1 + Z\mathbf{c}_2 \text{ where } Z \sim \text{Bern}(\alpha) \quad (10)$$

A third strategy, suggested for images in Magic3D [2], interpolates the DDM’s guidance weight. Unlike Magic3D, we amortize over guidance weights, reducing cost while providing continuous interpolation (not allowed via re-training on each weight). Specifically, we guide with:

$$\hat{\epsilon} = \epsilon_{\text{uncond.}} + (1 - \alpha)\omega_1\epsilon_{\text{prompt 1}} + \alpha\omega_2\epsilon_{\text{prompt 2}} \quad (11)$$

Here, the ω_1 and ω_2 are notations for the guidance weights for the predicted noise on the 1st and 2nd prompts respectively, which are fixed and equal in all experiments. This interpolates between using guidance on the first prompt, to guidance on the second prompt.

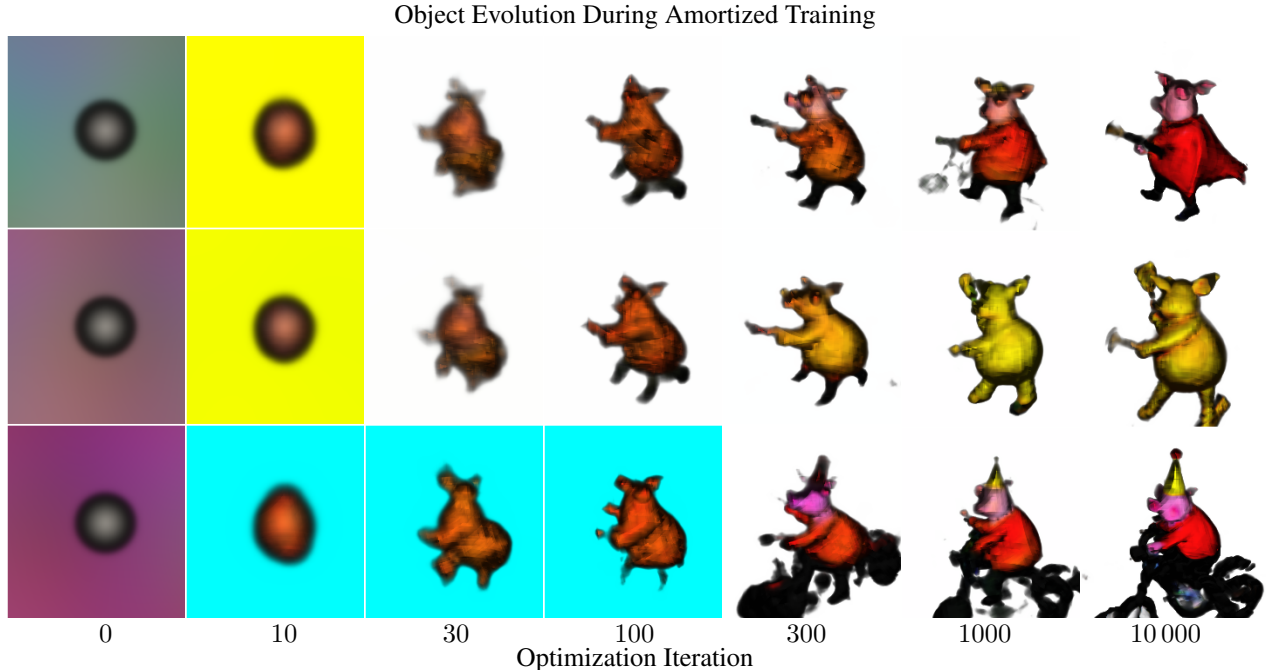


Figure 10: We show assorted training trajectories of the rendered objects during compositional training from Figures 6 and 2. *Left:* We visualize the initialization strategy described in Section B.1.9.

B.2. Compute Requirements

We implement our experiments in PyTorch [70].

B.2.1 Per-prompt Optimization

We do all per-prompt training runs on an NVIDIA A40 GPU, with a batch size of 32 for up to 8000 steps or ~ 4 hours. DF27 (Figure 6, left) use 27 runs, while the compositional prompts (Figure 8) use 50 or 300 subsampled runs respectively. Each training step costs ~ 1 second.

B.2.2 Amortized Training

Memorization & generalization: When amortizing many prompts, we use multiple GPUs to train with a larger batch size, causing amortized and per-prompt training to have different update costs. So we report the total rendered frames to compare compute accurately. Updates are roughly 1 second in each setup.

We perform the DF27 (Figures 6, 11) and DF411 (Figures 9, 14) runs on 8 NVIDIA A40 GPUs, each with a batch size of 32. We train DF27 for 13 000 steps (~ 4 hours) and DF411 for 100 000 steps (about a day).

The compositional runs (Figures 2, 6, 8) were performed on 4 NVIDIA A100 GPUs, with a batch size of 32 per GPU, for 40 000 steps or about 10 hours.

Interpolations (Figure 3): We use a single NVIDIA A40 GPU as in per-prompt training.

Finetuning (Figure 17): We use a single NVIDIA A40 GPU as in per-prompt training.

B.2.3 Inference

At inference – delineated from training in Figure 4 – we generate grid parameters in < 1 second and render frames in real-time due to our small final NeRF ν and efficient point-encoding γ . We use more ray samples at inference than training due to negligible cost and enhanced fidelity. Modulation generation occurs once and is reused for each view & location query, creating negligible overhead with many views or high-resolution images. During training with 1 view and image size 64 (batch size 8), hypernet modulations introduced an overhead of 24% more time per iteration, which could be avoided if our weights do not need to be generated. With 1 view and image size 256 (batch size 1) in inference, the modulation introduced an 11% overhead in rendering time, dropping to $< 1\%$ with 30 views.

C. Results

C.1. Additional Experiments & Visualizations



Figure 11: Our method, ATT3D, uses a single model to produce 3D scenes with varying geometric and texture details from the set of 27 prompts in the main DreamFusion paper [1]. The quality is comparable to existing single prompt training and requires far fewer training resources (Fig. 6).

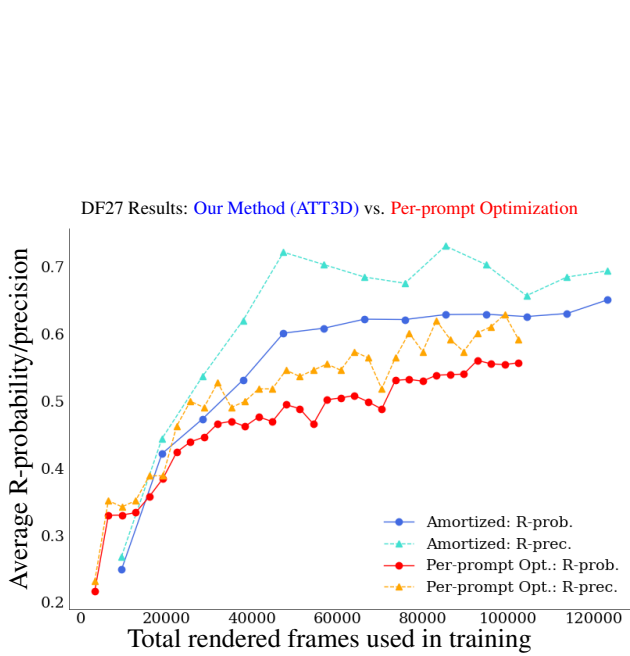


Figure 12: We show the same plot as Figure 6 with the addition of R-precision. **Takeaway:** Results with R-precision are similar to — but noisier than — R-probability when we have few prompts.



Figure 13: We qualitatively compare the unseen “testing” results from the various training strategies in Figures 6 and 2, with our method in blue and baselines in red. Notably, amortized requires no test time optimization, while fine-tuning uses a small amount, and per-prompt uses a large amount to tune from scratch.

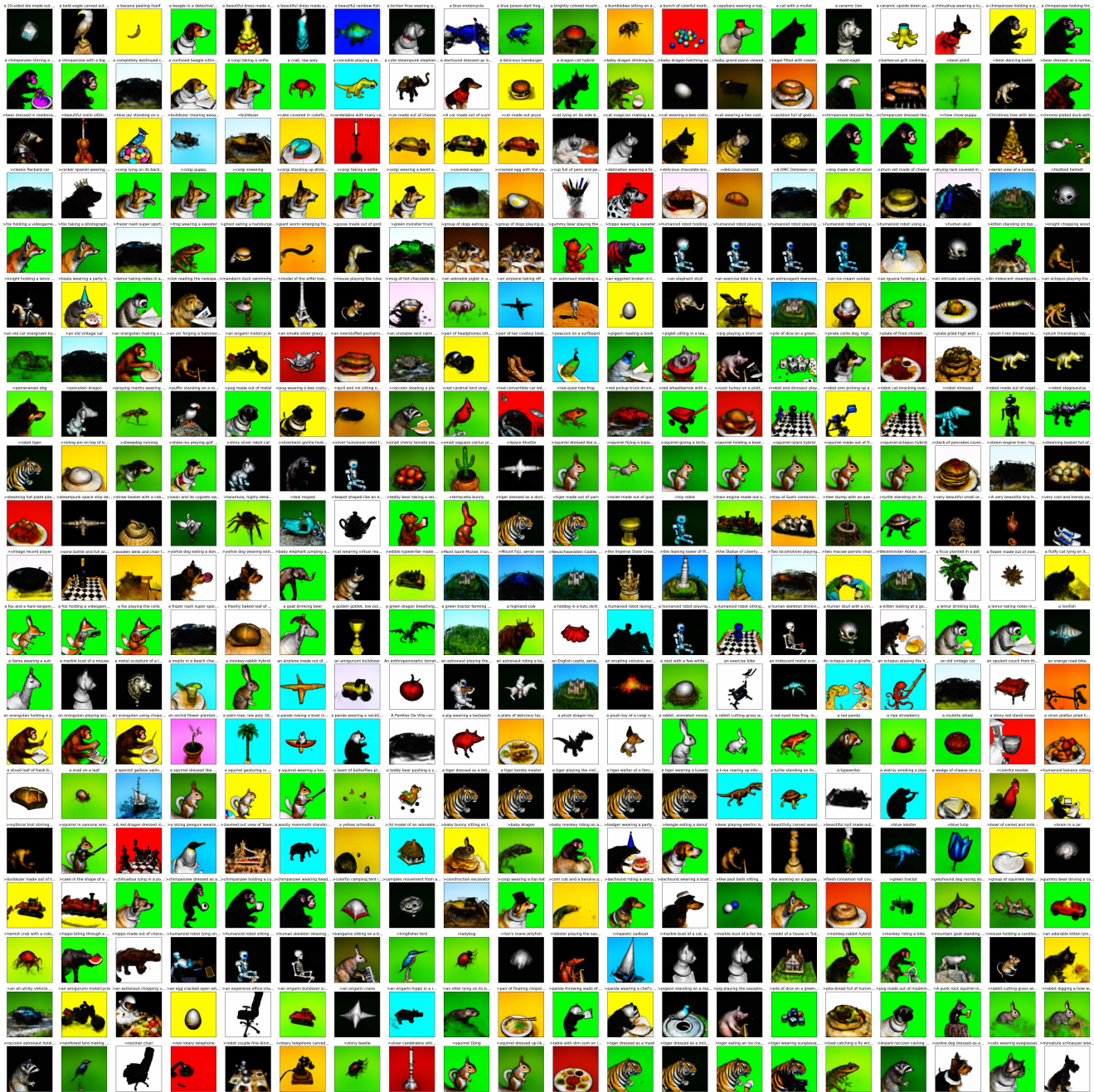


Figure 14: We show full results from our method on the DF411 prompt set, which we truncate for Figure 9. There are various examples of the model re-using object components across prompts – see Figure 15.

Component Re-use in DF411

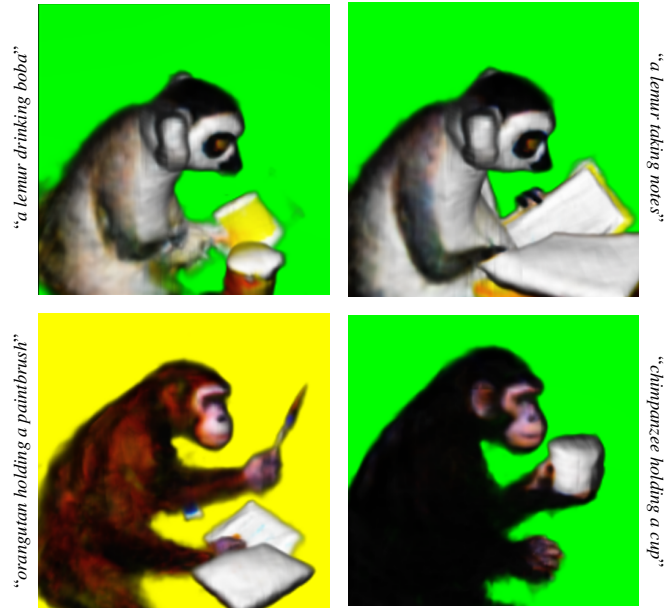
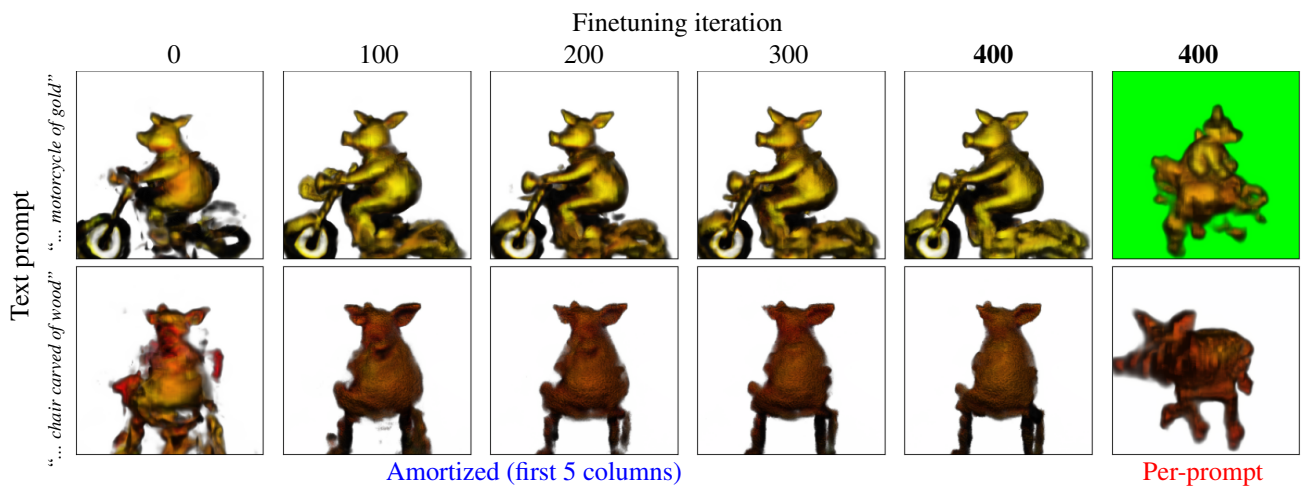


Figure 15: We show examples of prompts in which our model (from the DF411 run in Figures 9 and 14) re-uses components, showing a means by which amortization saves compute. *Top*: The lemur is re-used with different activities. *Bottom*: The orangutan is re-colored to a chimpanzee and given a different activity.



Figure 16: We investigate generalization on the DF411 run (App. Fig. 14). *Left*: Generalization to interpolated embeddings, which produces suboptimal results that we improve by amortizing over interpolants as in Figure 3. *Right*: Generalization to compositional embeddings. **Takeaway**: The generalization is promising, yet could be improved, motivating training on large compositional sets in Figures 6 & 8, and training on interpolants as in Figures 3, 18, 19, & 20.



Various strategies on “a pig wearing medieval armor holding a blue balloon”

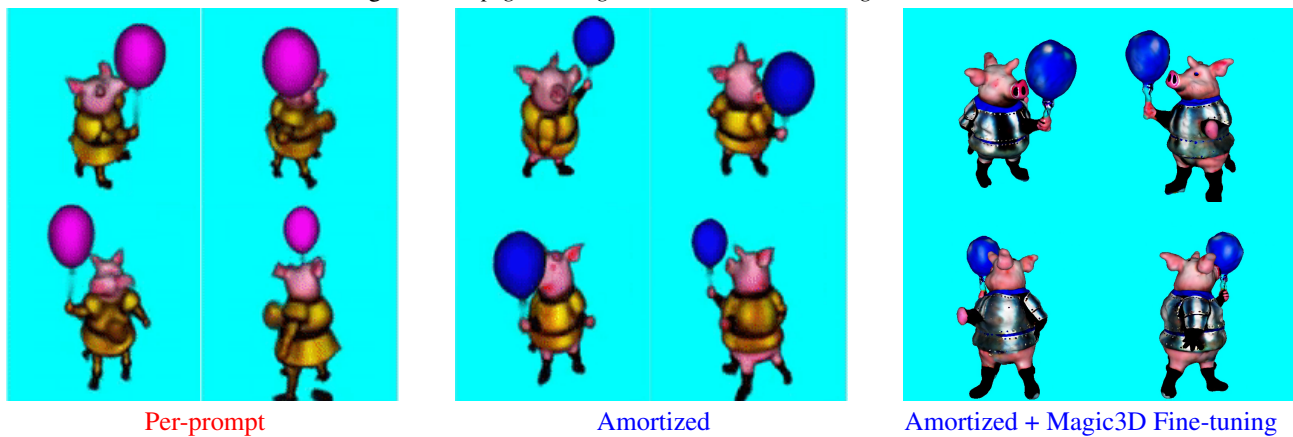


Figure 17: We display the results of finetuning held-out, unseen testing prompts from Fig. 2. *Top*: For amortization, we finetune from the final optimization value, while for per-prompt, we finetune the model from a random initialization. We achieve higher quality with fewer finetuning updates. *Bottom*: Per-prompt optimization fails to recover a blue balloon, and can not be recovered with finetuning. In contrast, amortized optimization recovers the correct balloon and can be fine-tuned using Magic3D’s second optimization stage [2].

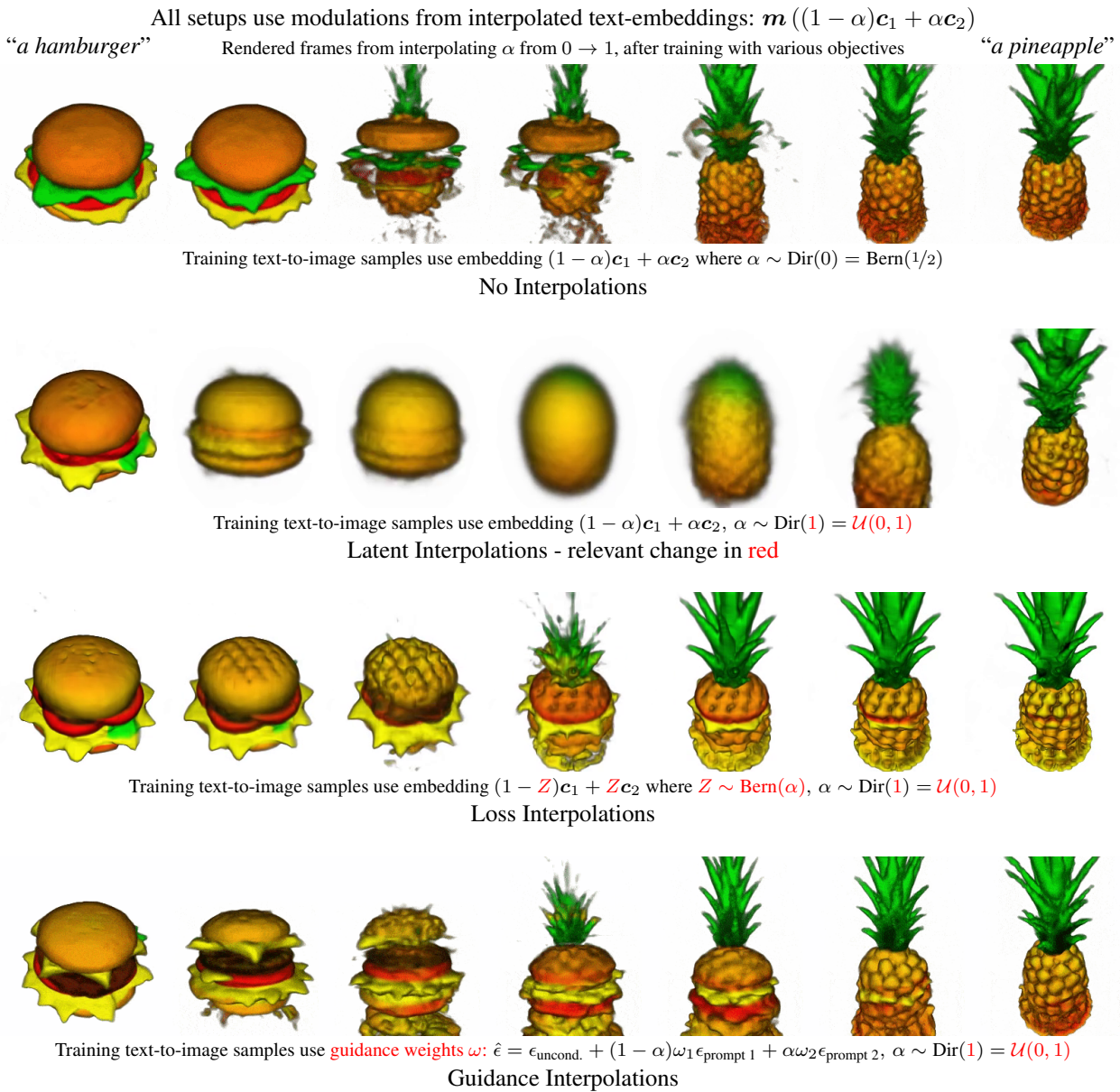


Figure 18: We contrast amortizing over different types of interpolations as described in Section B.1.14. For all examples, we give the mapping network m the interpolated embedding $(1 - \alpha)c_1 + \alpha c_2$. However, we vary the embedding used by the text-to-image model. **Takeaway:** We can amortize over various training methods to produce qualitatively different results. *Top:* We use no interpolants during training, which can just dissolve between the endpoints. *Latent Interpolation:* We simply interpolate between the latent embeddings used for image sampling. *Loss Interpolation:* We interpolate the loss function used in training between the prompts, producing objects simultaneously solving both losses. *Guidance Interpolation:* We interpolate the guidance weight applied to the prompts, as explored in Magic3D (without amortization) [2].

Rendered Frames Interpolating α from $0 \rightarrow 1$, where training $\alpha \sim \text{Dir}(\kappa)$ with varying κ

“a wooden pirate ship”

“a rubber life raft”

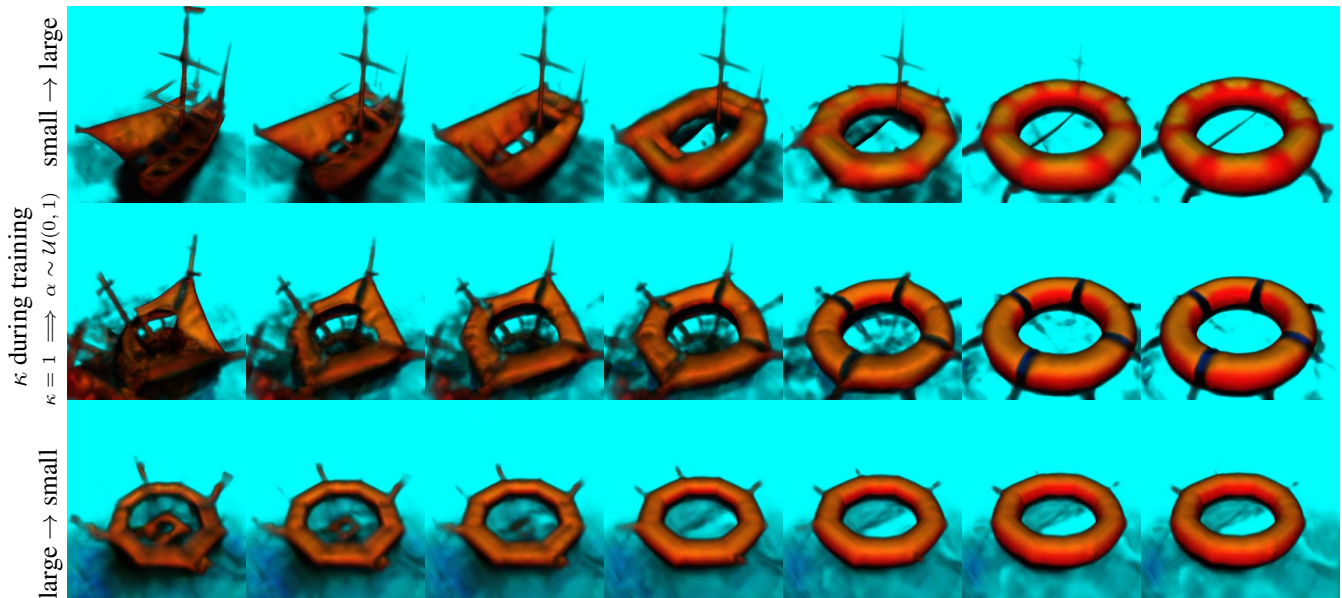


Figure 19: We display the results for differing strategies for changing the concentration parameter κ for the distribution of the interpolation weights α . Note that a concentration of $\kappa = 1$ is simply a uniform distribution: $\text{Dir}(1) = \mathcal{U}(0, 1)$. For both results, we train for 5000 steps with an initial concentration κ , which we then change for the final 5000 steps. **Takeaway:** The initial shapes learned strongly influence subsequent training, and a “large” concentration κ focuses on the midpoint, while a “small” concentration focuses on the endpoints. If we want the original prompts in the interpolation, then we should start with κ small, while if we desire a steering-wheel-life-raft satisfying both losses, we should start with κ large.

“... an adorable cottage with a thatched roof”

“... a house in Tudor Style”



“a frog wearing a sweater”

“a bear dressed as a lumberjack”



“... a majestic sailboat”

“a spanish galleon...”



“a ficus planted in a pot”

“a small cherry tomato plant...”



“a baby dragon”

“a green dragon”



“jagged rock”

“mossy rock”

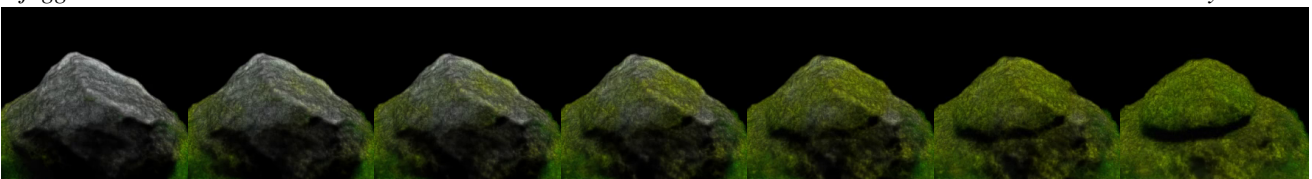


Figure 20: We include additional results for using our method to amortize over (loss) interpolants between prompts. We alternate between a fixed and varied camera view. We show examples of varied buildings, characters, vehicles, plants, landscapes, or a simple animation of “a baby dragon” aging into an adult.